Joerg Bellmann, Eckhard Beyer, Joern Lueg-Althoff, Soeren Gies, A. Erman Tekkaya, Sebastian Schettler, Sebastian Schulze

Targeted Weld Seam Formation and Energy Reduction at Magnetic Pulse Welding (MPW)

Abstract: Magnetic pulse welding is based on the high velocity impact of two joining partners and a promising technology especially for the joining of dissimilar metallic components. Under proper conditions, a solid-state bond forms at the overlapping interface that is typically at least as strong as the weaker base material. However, high thermal and mechanical loads act on the tool coil and provoke a limited lifetime. Furthermore, the prevalent magnetic fields obstruct a comprehensive process monitoring with conventional means. In this manuscript, approaches for reducing the load on the tool coil without compromising the joint quality are presented. This is obtained by an adaption of the coil geometry and the application of a boundary layer on one of the joining partners. Moreover, a new measuring system taking advantage of the naturally occurring impact flash is evaluated and successfully applied for the process development and detection of process disturbances.

Keywords: magnetic pulse welding, surface coating, energy reduction, torsion testing

DOI: *10.17729/ebis.2017.5/10*

Introduction

The reduction of the mass of products and structures is an ongoing challenge in various commercial sectors like automotive or aerospace industries. For lightweight design, the choice of a component's material is usually based on its specific function and contribution to the structure's mass, irrespective of its compatibility to the other parts. This leads to a material mixture and thus to the rising necessity of joining different or even dissimilar materials. Conventional fusion welding techniques can come to their technological limits when the metallic parts to be joined have strongly different thermo-physical properties like melting points and thermal conductivities. Often, brittle intermetallic compounds promote cracking and limit the overall joint quality. Solid-state joining techniques like impact welding can be a viable alternative. In these processes, the weld

Joerg Bellmann (M. Sc.), Eckhard Beyer (Prof. Dr.-Ing. habil.) – Technische Universität Dresden, Fraunhofer IWS Dresden, Germany; Joern Lueg-Althoff (Dipl.-Wirt.-Ing.), Soeren Gies (Dipl.-Wirt.-Ing.), A. Erman Tekkaya (Prof. Dr.-Ing. Dr.-Ing. E.h.) – Institute of Forming Technology and Lightweight Components, TU Dortmund University, Germany; Sebastian Schettler (Dipl.-Ing.), Sebastian Schulze (Dr.-Ing.) - Fraunhofer IWS Dresden, Germany

formation is not accompanied by an excessive heating of the parts. Thus, heat induced defects are largely avoided. Magnetic pulse welding (MPW) is such a solid-state welding technique. Here, at least one of the joining partners, the "flyer", is accelerated by the magnetic pressure, which forms in the gap between the workpiece and a tool coil during the rapid discharge of energy through this coil. After overcoming the standoff between the two joining partners, the flyer collides with the stationary "parent" part at impact velocities of several hundred meters per second. Under adequate conditions, typically a flash occurs, which can be recorded and correlated with the welding result [1, 2]. The flash accompanies the jetting effect, which cleans and activates the surfaces of the joining partners so that a weld can be established under the action of the prevalent high impact pressures. Typically, MPW processes are characterized by the collision angle β and either the impact velocity v_i or the axial velocity of the collision point v_c. Following the practice of explosion welding processes, proper MPW process conditions are typically plotted in so called welding windows in the dimensions β and v_c. The interface between parts joined by impulse welding often features a wavy appearance (Fig. 1c), which illustrates the high stresses and strains during the collision process. However, also sound welds with a straight interface have been reported [3].

In previous investigations, the fabrication of driveshafts by MPW has been investigated. Flyer tubes made of aluminum were used and for the parent rods aluminum as well as steel was tested. Circumferential weld seams with an axial length of 4 mm could be manufactured. The interface showed waves with an amplitude up to 10 µm. The low heat input prevented the formation of heat affected zones (HAZ). Consequently, the structures made by MPW had a higher quasistatic strength compared to parts joined by laser beam welding or electron beam welding. The cyclic strength of the weld seam turned out to be higher than the strength of the weaker base material so that cracks occurred in the aluminum [4].

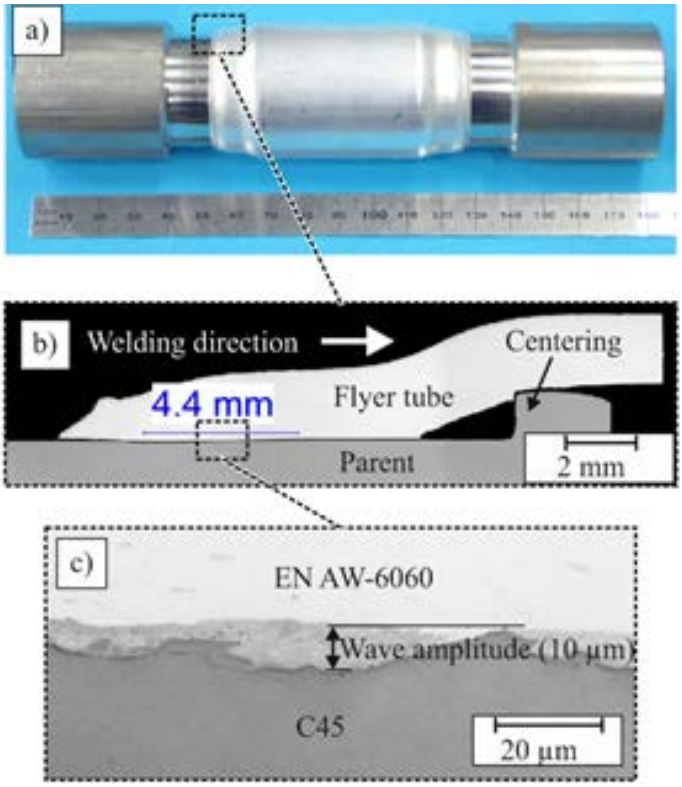

Fig. 1. a) MPW-joint between aluminum and steel, b) polished cross section of the welded zone with 4.4 mm weld length, c) wavy interface between aluminum and steel (according to [4])

However, several shortcomings of the process exist, which are opposed to the application of MPW processes in industrial line production. The necessary high current densities cause high thermal loads on the tool coil. This Joule heating is influenced by the amount of discharge energy and the cycle time in sequential processes [5]. The higher the energy and the shorter the cycle time, the higher the heat input and the resulting tool coil temperature. Moreover, the magnetic pressure in the gap between flyer and coil leads to shock loading conditions. The combination of thermal and mechanical shock loading limits the lifetime of MPW tool coils significantly. Thus, the reduction of the discharge energy or tool coil current, respectively, is a promising approach to work against these effects.

The objective of the present investigation is the reduction of the tool coil current with

unchanged weld quality. To reach this goal, two different strategies were pursued and the results were compared to the reference setup presented in [4], where a discharge energy of 13.5 kJ lead to 4 mm long weld seams. In a first step, the geometry of the tool coil was adapted in order to optimize the magnetic pressure profile acting on the flyer and to decrease the current density in the coil. Moreover, an intermediate layer was applied on one of the joining partners prior to the MPW process. This approach was suggested by Yablochnikov [6] and was tested by Bellmann et al. for the current material combination [7, 8]. It was reported that nickel coatings on steel parent parts could effectively *enlarge* the weld seam length during MPW with aluminum flyer parts with constant discharge energy. Following these experiences, nickel coatings were used as intermediate layers in the present work to reduce the necessary input energy and evaluate the effect on the joint strength in comparison with the uncoated samples. The characterization of the joint quality was done by quasistatic and cyclic torsion testing, adapted to the anticipated loading conditions in the service life of driveshafts. The location and propagation of cracks during these tests was studied.

For process monitoring, the newly presented optical technique based on the recording of the impact flash was used. This technology was developed and introduced by the authors [1] and was correlated with the charging energy for the present investigations. For each joining experiment, the flash appearance time was recorded with this tool in order to identify possible process disturbances.

Experimental setup

Joining setup

Experiments were performed with flyer tubes made of aluminum EN AW-6060 T66. The tubes had an outer diameter of 40 mm, a wall thickness of 2 mm, and a length of 70 mm. The quasistatic yield strength was determined by tube tensile tests with approximately 222 MPa. The inner parent shafts had a diameter of 40 mm, a length of 60 mm and were made of steel C45 (see Fig. 2). The necessary initial standoff between the joining partners was achieved by machining and polishing a 20 mm long joining area with a diameter of 33 mm and a roughness R_a below 1 µm. For selected steel specimens, a 5 µm nickel coating was electroplated in the joining area. The chemical compositions of the materials are listed in Table 1.

Table 1. Aluminum EN AW-6060 alloy composition [9] and steel C45 (1.0503) alloy composition [10]

Flyer part EN AW-6060, T66		Parent part C45 (1.0503), normalized	
Element	Weight %	Element	Weight %
Mg	0.35-0.6	C	0.42-0.5
Mn	≤0.1	Mn	0.5-0.8
Fe	0.1-0.3	P	<0.045
Si	0.3-0.6	S	<0.045
Cu	≤0.1	Si	<0.4
Zn	≤0.15	Ni	<0.4
Cr	≤0.05	Cr	<0.4
Ti	≤0.1	Mo	<0.1

The joining partners were positioned coaxially inside a single turn tool coil made of CuCr1Zr as depicted in Figure 2. In this sketch, the definitions of the azimuthal measurement positions and the unavoidable axial slot in the tool coil are shown. The geometrical definitions and the position of the optical measuring system for the detection of the high velocity impact flash are given in Figure 3. Only 6 mm from the maximum working area of 10 mm was used for acceleration of the flyer. This so-called "working length" ensures optimum welding conditions. A pulse generator B_{max} MPW 50/25 was used for the storage and supply of the necessary discharge energy. Its characteristic values are listed in Table 2. When the capacitor of the pulse generator is discharged via the tool coil in a damped, sinusoidal current (see exemplary course in Figure 4), the magnetic pressure accelerates the flyer radially. After the joining

standoff the flyer collides with the parent. This impact is accompanied by a flash, which can be recorded by collimators. Therefore, the centering structure at the parent part (see Fig. 1 b)) had to be removed in order to gain optical access to the joining zone. Especially the flash appearance time $t_{f,start}$ in Figure 4 was used for process analysis.

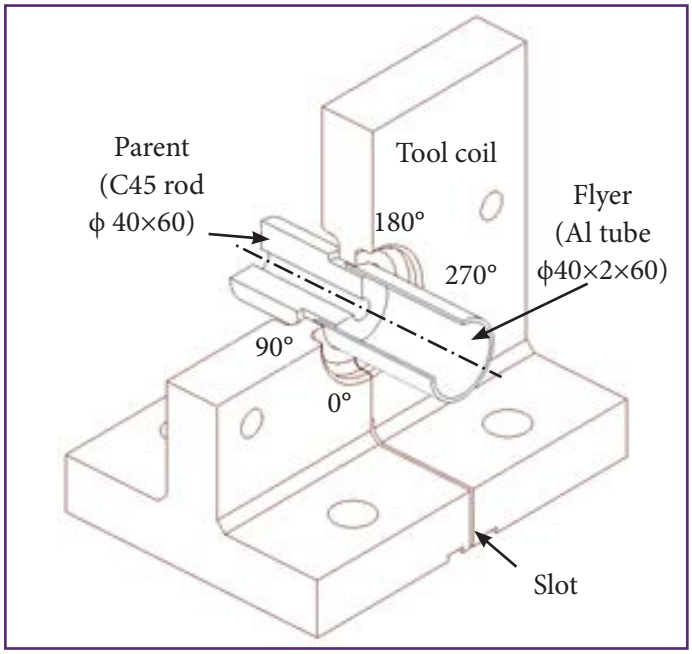

Fig. 2. Sectional view of the joining setup without insulators and centering parts (all values in mm)

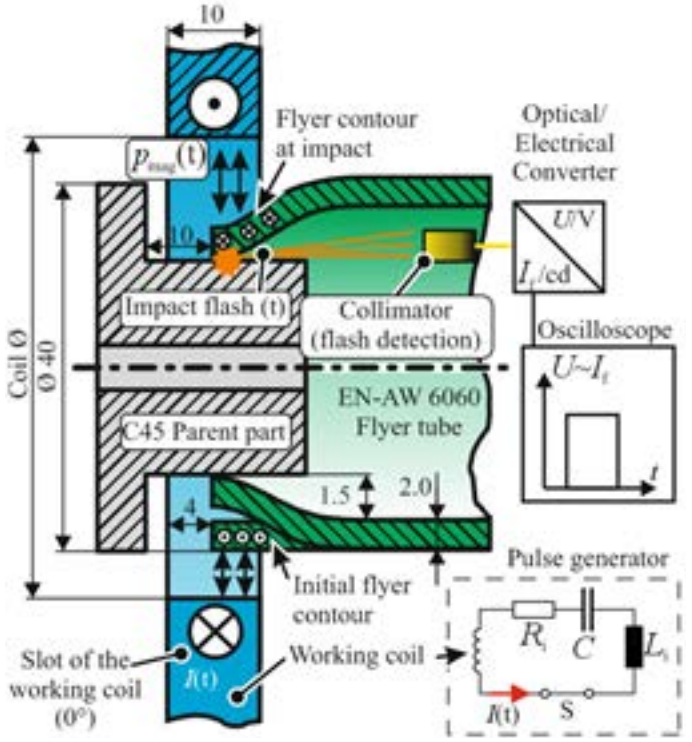

Fig. 3. Geometrical definitions of the joining setup and measurement system for flash detection (not true to scale, all values in mm)

During the process adjustment, the circumferential weld quality was verified by a manual peel test [1]. In order to identify the lower energy limit, the charging energy was gradually decreased after each successful weld until a non-weld was detected. With the knowledge of the minimum discharge energy for a circumferential weld, samples for torsion testing were manufactured, see Fig. 1 a. Each sample consisted of an aluminum tube connected to two steel rods with the previously described geometries. The two weld seams between the aluminum tube and the steel rods were manufactured successively. The length of the tube was reduced compared to real driveshafts to avoid buckling and to assure the ability to test

Table 2. Characteristics of the pulse generator Bmax MPW 50/25

Setup	Value	Unit
Capacitance	160	µF
Resistance (short circuit)	2	mΩ
Output stage inductance (short circuit)	58	nH
Maximum charging energy	32	kJ
Applied charging energy – E	5.8 … 8.0	kJ
Corresponding maximum tool coil current I_{max} (E)	≈ 35·E(kJ) + 236	kA
Discharge frequency with coil and workpieces - $f_{discharge}$	20	kHz

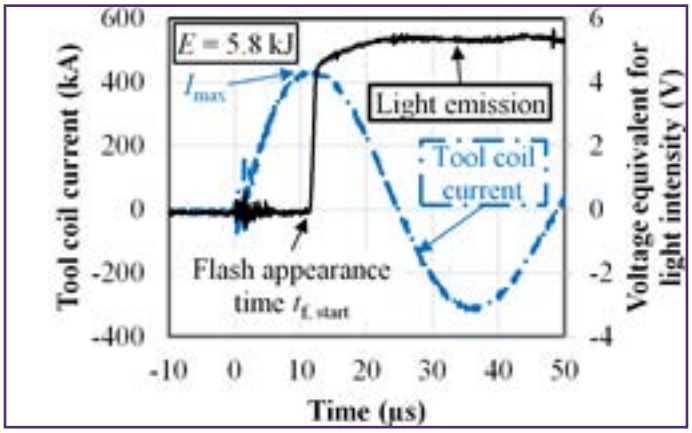

Fig. 4. Example of tool coil current and light intensity vs. time

the weld seam itself. The minimum overall sample length was limited by the mounting ability of the rods' ends in the clamping system of the testing machine and was set to 170 mm. The clamping zone in the torsion testing machine is ϕ40 × 40 mm on each side. Again, the flash appearance time tf,start was recorded for every experiment.

Metallographic investigations

Metallographic investigations were performed to get deeper insights into the processes that happened in the joining zones with and without intermediate nickel layer. Therefore, cross-sections polishes of selected samples at the 180° location (see Fig. 2) were prepared. The weld seam lengths, the shape of the interfacial waves and the hardness were determined and compared. In addition, the geometry of the parts was measured with regard to deformations and presumed energy input. The position of the failure during quasistatic and dynamic testing was determined for the experiments with and without coating. In this context, also the hardness of the material in the joint interface was measured.

Mechanical testing

Shear tests were performed to measure the weld length. For every joining configuration, three welds underwent a shear test depicted in Figure 5. Therefore, the flyer was machined in order to apply a shear ring on the parent. After the flyer and the shear ring were removed, the weld length lw was identified by measuring the length of aluminum residues on steel. This was done at four positions according to Figure 2. The weld length was significantly reduced at the coils slot between the azimuthal angle of 345° and 15°, while the remaining circumference showed similar weld lengths. Thus, the mean weld length of each sample was weighted according to Equation 1.

$$l_{w,mean} = \frac{1}{12} l_w(0°) = \frac{11}{12} \frac{l_w(90°) + l_w(180°) + l_w(270°)}{3} \quad (1)$$

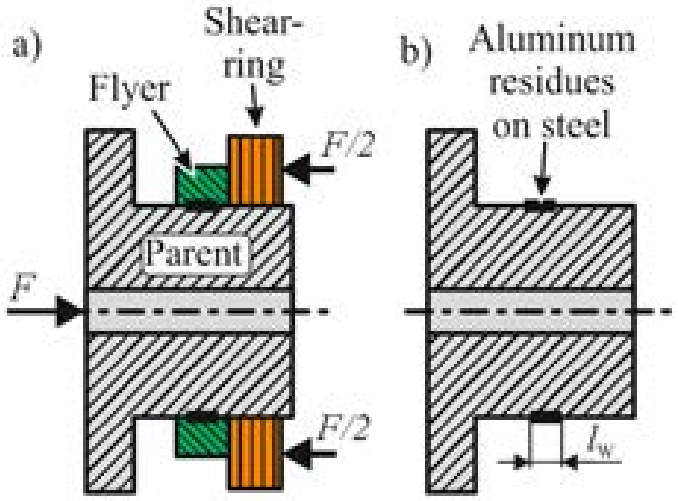

Fig. 5. a) Shear test and b) evaluation of the weld length l_w

A servo-hydraulic axial-torsional testing machine from Inova was used for the evaluation of the torsional strength. During all tests, the axial force in the samples was controlled to zero. For quasistatic testing, the torque was measured while a constant angular velocity of 10°/minute was applied, resulting in a torque-angle curve. The cyclic testing was performed according to DIN 50100:2016-12 by using an alternating torque (stress ratio R = -1) with constant load amplitude. The test frequency was set to 20 Hz and a maximum number of two million load cycles was used as stop criterion [11]. The results of previous tests were used to set the initial torque amplitude to 119 Nm [4] and the following steps to 131 Nm and 143 Nm. The evaluation of the torque amplitude with 50% failure probability was reached by using the so called staircase test method. Cracks in the samples were indirectly identified by monitoring the angle amplitude during the cyclic testing. The tests were aborted and the samples were classified as failed, if a limit of ±0.01° was exceeded. For each sample, the aluminum's outer surface in the joining zone was analyzed in detail with optical microscopy in order to identify any cracks.

Results and discussion

Influence of the coil geometry and coating

The aim of this work is the decrease of the maximum tool coil current and charging energy,

respectively. In a first step, the gap between the coil and the flyer was reduced from 1 mm to 0.5 mm in order to achieve the same magnetic flux with less tool coil current. Using the equations from Psyk et al. [12, pp. 106–112] for the setup number 1 in Table 3 (according to [4]) leads to a magnetic pressure of 608 MPa in the middle of the coil's concentration zone at the current maximum of 656 kA without considering the geometrical effect of the working length. If the gap between coil and flyer is reduced to 0.5 mm, the same pressure can be derived with only 645 kA. Experiments with setup number 2 showed that even a reduction to 517 kA generates a circumferential weld seam proved by manual peel testing. Probably, the forming behavior of the flyer was improved with the ϕ 41 mm coil at the same time. This results in a significant reduction of the magnetic pressure, proved by the delay of the flash appearance time. In a third setup, the parent part was electroplated with a 5 µm thick layer of nickel. This surface treatment *reduced* the necessary tool coil current for asound weld to 438 kA or 5.8 kJ charging energy, respectively and *increased* the weld length at the same time. Table 3 shows the further increased flash appearance time due to the reduced energy input. Trials for joining an uncoated parent part with the flyer according to setup number 3 were performed, but no circumferential weld was obtained.

During the joining of the samples that were intended for the torsions tests, the flash detection method was used to identify possible disturbances in the joining setup. Within 20 welds, the mean values for tf,start were 10.6 µs (SD=0.5 µs) for 8 kJ charging energy respectively 12.2 µs (SD=0.7 µs) for 5.8 kJ. This is in good correlation with the results shown in Table 3 and indicates a good repeatability of the process.

Morphology of the joining zone

Setup 2 and 3 differed in two parameters: the charging energy and the intermediate layer. From earlier experiments it is known that the intermediate nickel layer influences the waviness of the joining zone even with constant charging energy [7]. Consequently, some of the effects in the morphology of the joining zone that are depicted in Figure 6 cannot be attributed to one of the both factors without a doubt. For example, the reduced depth and length of the indentation zone in the steel rod are *probably* related to the reduced energy input, but might also be a result of the damping properties of the intermediate nickel layer as suggested by Verbraak et al. [13]. In contrast, the larger flyer thickness next to the initial point of impact *clearly* indicates less material flow to the left direction due to the reduced energy input. The flyer thickness in the right corner of Fig. 6 d) or Fig. 6 e), respectively, does not differ between both charging energies, since this section is outside of the tool coil's concentration zone during welding.

The detailed metallographic analysis in Figure 6 reveals that:

Table 3. Influence of the coil diameter and parent coating on the minimum tool coil current for a circumferential weld

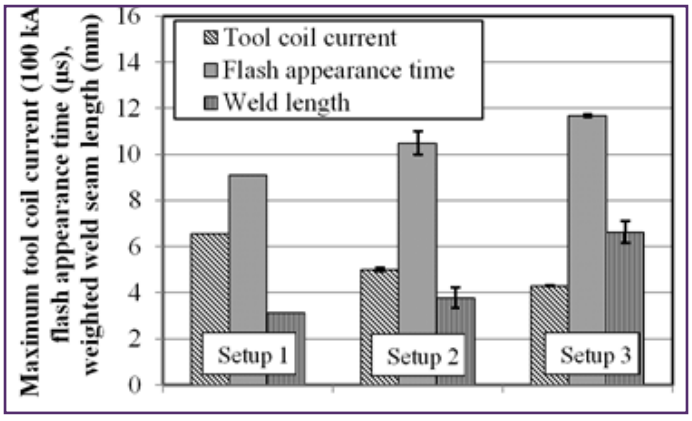

Setup number	1	2	3
Number of tests	1	3	3
Coil ϕ (mm)	42	41	41
Coating	w/o	w/o	5 µm nickel
Charging voltage (kV)	13	10	8.5
Charging energy (kJ)	13.5	8.0	5.8

1. The middle and end zones of the uncoated samples include waves with a maximum height of 10 µm. The material that was pushed into the pockets of the interface has a hardness above 700 HV0.01 (Fig. 6 c)) and, thus, is much harder than both base materials (Fig. 6 a)). Probably, an intermetallic phase was formed from aluminum and iron.
2. The weld zone with the intermediate nickel layer is almost two millimeters longer than the one of the uncoated sample and shows no waviness. One reason might be the reduced energy input; another explanation is the increased hardness of the nickel layer compared to the steel surface. Thus, the resistance of the parent part against the penetration of the flyer is increased as well. The intermediate layer is not disrupted at any point. In the middle of the welded zone it is probably partly melted and intermetallic phases with hardness values above 600 HV0.01 were formed from aluminum and nickel.

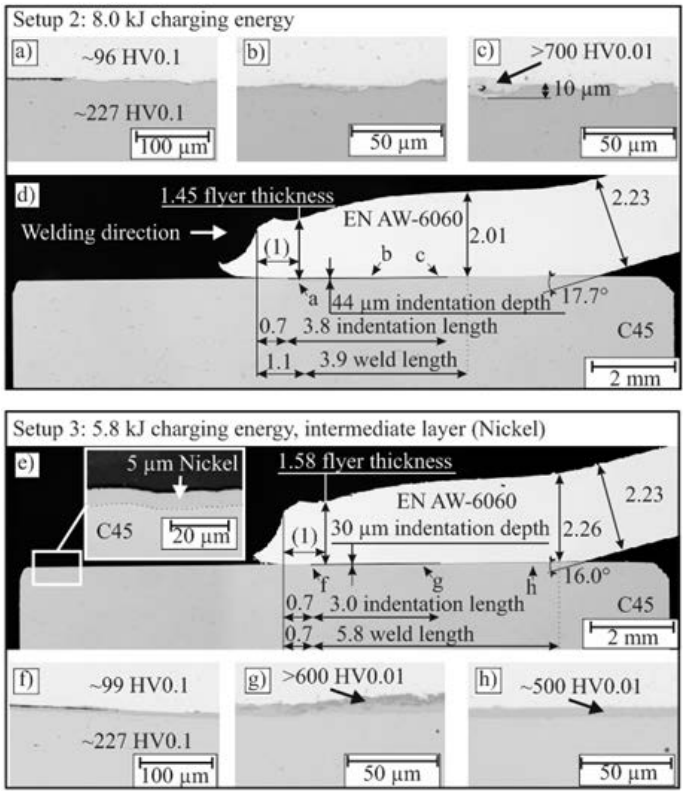

Fig. 6. Polished cross sections showing the joining zones at the 180° positions of the uncoated sample (a-d) and the effect of the intermediate nickel layer (e-h) (all values in millimeter, if not indicated)

These statements point to the conclusions that welding between aluminum and nickel requires less impact energy than MPW of aluminum and steel. Probably, the amount of plastic deformation in the weld zone is not the only relevant parameter, since welding was achieved also without any deformation of the parent or the nickel layer, respectively (see Fig. 6 h)). The intensity and the length of the high velocity impact flash are almost identical for both setups. Thus, a similar surface activation can be presumed and the positive effect of nickel is probably related to metallurgical phenomena. For instance, the reaction of nickel and aluminum is exothermic and requires less activation energy than the reaction of aluminum and iron. Thus, it is used as a heat source also for other joining applications in the shape of so called Reactive Multilayer Systems [14, pp. 102–103]. Furthermore, the crystal structure is cubic face centered for both nickel and aluminum, which probably supports the atomic bonding.

MPW is generally categorized as a welding process without heat affected zones due to the very low heat input. Hardness measurements

Table 4 Hardness distributions at the 180° position after the joining process (HV0.1 mean values and SD for each position)

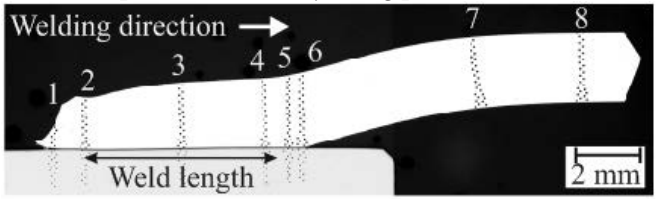

Position number	1	2	3	4	5	6	7	8	Base material aluminum
w/o coating	91±13	94±5	92±5	93±5	93±4	92±4	90±3	86±4	84±3
Ni coating	94±6	96±5	95±3	95±4	96±4	93±3	89±4	87±3	

in the vicinity of the joining zone at different axial locations according to Table 4 verified this statement. Furthermore, the hardness distribution across the complete aluminum tube was evaluated. The base material of the aluminum tube has a hardness of (84±3) HV0.1. Due to the radial compression of the tube during the acceleration phase the hardness was increased depending on the amount of deformation. For example, position number 7 is just slightly deformed and thus softer compared to position number 3 in the middle of the welded zone. This effect appeared for both batches and there is no significant influence of the charging energy on the quantitative hardness values.

Torsional strength of uncoated and coated parts

Torsional tests were performed in order to investigate the influence of the nickel coating on the joint strength. As shown in the previous chapter, the coated samples differ from the uncoated batch in the weld seam length as well as the flyer's geometry after the welding process due the reduced energy input. Furthermore, the stress along the weld seam is inhomogenous distributed due to the overlapping joining configuration. Thus, the calculation of a comparable weld seam strength is hard to obtain with this test setup. Nevertheless, a comparison of the global part's performance is valid due to the similar sample geometry.

Quasistatic tests

The results of the quasistatic tests are shown in Figure 7. The torque is plotted against the angle of twist for three nickel coated and three uncoated samples.

Both batches show a similar stiffness within the linear-elastic region. The coated samples differ from the uncoated ones in a slightly lower maximum torque value. Much more important is the fact that samples with an intermediate layer made of nickel withstand a 8° higher angle of twist until failure, which is divided into 4° among each joined area. For every tested sample, the weld seam passed; no buckling occurred and a crack was initiated near the end of the weld seam along the circumference of the tube, see Fig. 8. Metallographic analysis of the tested samples showed no evidence of separation or surging within the joining area. Thus, the quasistatic strength of the weld seams themselves was higher than the strength of the aluminum tubes in both configurations.

Hardness measurements of the tested aluminum tube cross sections were performed (see Table 5). The tube material between positions 3 and 8 is significantly hardened during the quasistatic torsion test compared to the unloaded samples in Table 4. Furthermore, the hardness of the sample joined with 8 kJ charging energy obviously increased in the area of the crack locations and kink of the tube (positions 5 and 6) compared to the low-energy sample. The comparison of the flyer thicknesses at the end of the joining zone for both batches

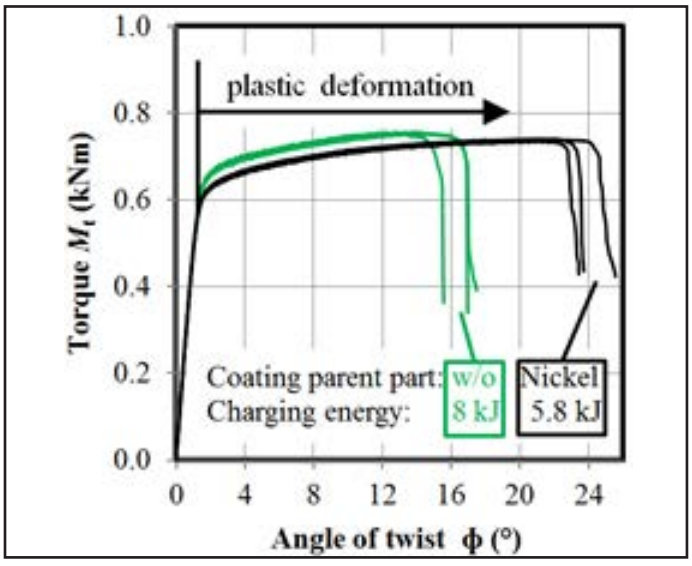

Fig. 7. Comparison of uncoated and Ni-coated samples in quasistatic torsion tests

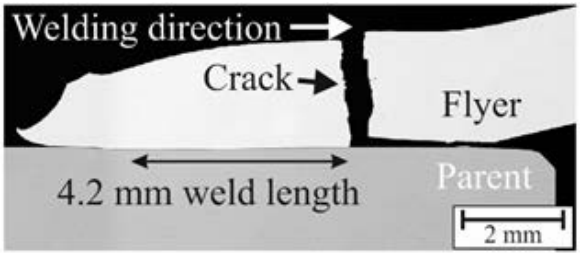

Fig. 8. Polished cross-section of an uncoated sample after quasistatic torsion testing

(see Fig. 6 d) and e)) revealed a 0.25 mm higher value for the sample from setup 3 (5.8 kJ charging energy), which is 12.5 % of the initial tube thickness. Thus, the load-bearing cross section is enlarged and the stress reduced, respectively. Consequently, this leads to lower hardening even for enlarged angles of twist. Furthermore, the angle between flyer and parent is smaller (see Fig. 6 d) and e)) resulting in a smooth transition with positive effect for the loading capacity or resilience.

Table 5. Hardness distributions at the 180° position after the quasistatic torsion test (HV0.1 mean values and SD for each position)

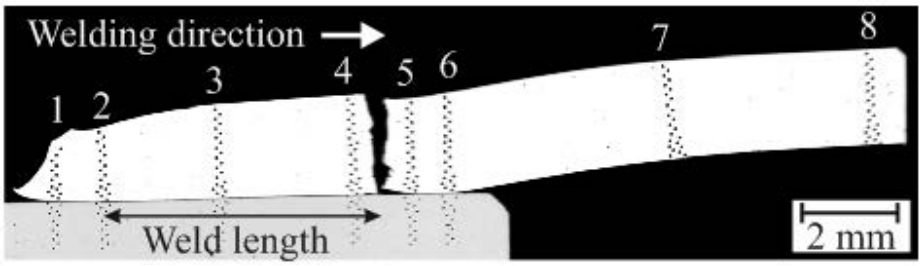

Position number	1	2	3	4	5	6	7	8
w/o coating	94±14	98±7	98±6	99±4	104±5	100±5	96±3	96±4
Ni coating	97±4	96±5	96±4	98±3	100±4	94±3	93±3	93±5

Cyclic tests

The results of the staircase test method for cyclic torsion loading are shown in Figure 9, while each batch included six samples. By analogy with the quasistatic tests, the first batch encompassed the uncoated samples joined at 8 kJ charging energy (setup 2). The torque amplitude of 50 % failure probability is 124 Nm with a standard deviation of 8 Nm. The samples with an intermediate layer made of nickel that were joined with 5.8 kJ charging energy in the second batch (setup 3) are almost at the same level. The comparatively high standard deviation is a consequence of the step interval that was defined with 10% for these dummy parts. This large step interval is probably not likely for the investigation of real component parts. Although the number of samples fits to the aim of *this* comparison, more samples would be necessary in case of *real* driveshafts.

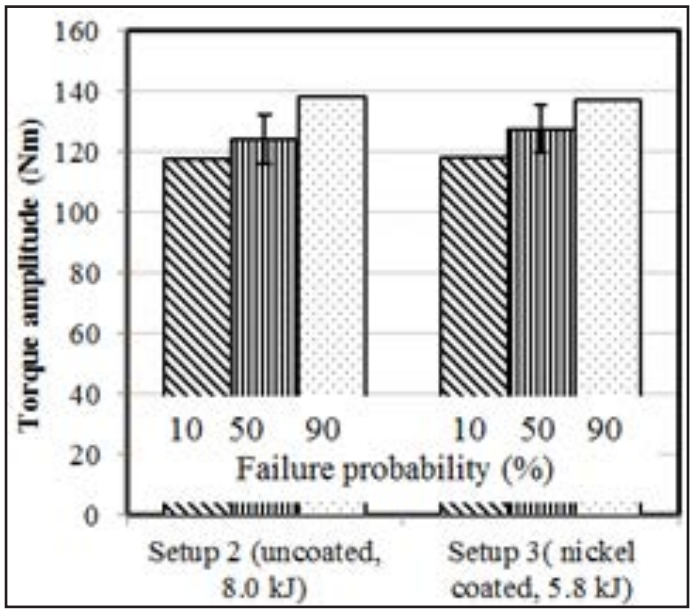

Fig. 9. Influence of the coating and charging energy on the torque amplitude with 10, 50 and 90 % failure probability

All tested samples underwent visual crack detection, while almost every failed sample obviously showed axial cracks in the tapered area of the aluminum tube. Those cracks either grew towards the center of the sample, partly in 45° direction or radially as indicated with "crack 1" in Fig. 10. Some of the passed samples that did not exceed the limit of angle of twist (0.01°) exhibited cracks, too. Those cracks were very small and could only be detected with the help of a microscope. Consequently, the deduced amplitudes for default represent just a cyclic strength within the defined truncation criterion (angle of twist <0.01° for two million load cycles). The fatigue limit is definitely *below* this value. The metallographic investigation also revealed a second crack initiation point that is located at the end of the welded zone as indicated with "crack 2" in Fig. 10. At this point, the notch effect caused a stress concentration and the crack grew 45° contrary to the welding direction. The flyer did not separate from the parent. Thus, the strength of the weld seam is higher compared to the aluminum base material in the

given load case. Intermetallic phases that were identified in Fig. 6 c) and g) do not affect the cyclic strength of the weld seams due to their low thickness and integration into the interface. Since crack 2 is not visible during the torsion tests, a statement regarding the time of crack initiation is not possible. Furthermore, only two of 24 cyclic tested joints were analyzed metallographically in order to detect failures in the style of "crack 2". The results show that the reduction of the charging energy with the use of

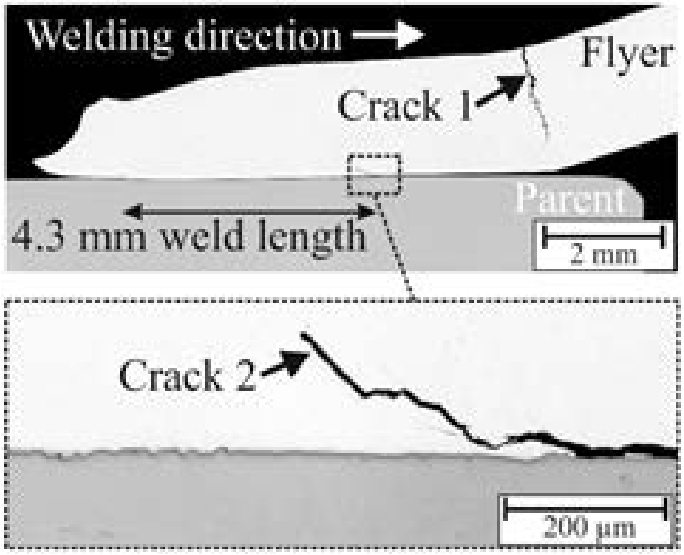

Fig. 10. Polished cross-section of an uncoated sample that failed during cyclic torsion testing

an intermediate nickel layer does not affect the overall strength of the sample. They also reveal that there are still possible improvements, e.g. the decreasing of the notch effects next to the joining zone and the deformed flyer.

Summary and Outlook

The present paper is about the optimization of the magnetic pulse welding process and focusses on two issues: the energy reduction and the process monitoring. Especially in large-scale production a lowered energy input is aimed to extend the lifetime of the tool coils. At the same time, a good weld quality and high strength of the joint has to be assured. To reach both aims, the experimental procedure followed two steps:

1. The tool coil diameter was reduced in order to achieve the same magnetic pressure with less energy. During the process optimization, the maximum tool coil current was reduced from 700 to 517 kA. With the help of the optical measurement system the collision time was monitored. Due to the decreased energy input, the collision time showed a delay, corresponding with a decrease of the impact velocity. Nevertheless, the weld quality was not affected, which points to the conclusion that the optimization of the tool coil was advantageous for the collision angle and front velocity, too.
2. The maximum necessary tool coil current was further decreased to 438 kA with an intermediate nickel layer that was applied on the parent part. With this setup, the weld length was even increased. First explanation approaches point to an improved thermal activation between nickel and aluminum and their similarity in the crystal structure.

The measurement system that was used for the process optimization and detection of process disturbances during sample preparation requires optical access to the joining zone in order to monitor the high velocity impact flash. Therefore, the centering structure at the parent part from previous investigations [4] had to be removed. It was found that the simplified parent contour did not affect the joining process or strength of the parts.

Samples were joined with reduced energy input according to both strategies and underwent quasistatic and cyclic torsion tests. If the magnetic pressure is decreased with the help of an intermediate layer, the flyer thickness in the areas with the critical load is larger. Thus, the angle of twist until failure can be increased as well during quasistatic torsion. In cyclic tests, notch effects at the end of the weld seam and the tapered flyer geometry lead to crack initiation and failure at the upper stress level of the step test method. These locations have to be optimized geometrically in order to increase the global performance of the magnetic pulse welded parts. Nevertheless, the cyclic loading capability does not differ significantly between

the uncoated and nickel coated samples. Failure occurred always in the base material of the aluminum tube and not in the weld. Thus, the application of an intermediate nickel layer on the parent part is a promising method to reduce the energy input when welding aluminum on steel.

Acknowledgments

This work is based on the results of subproject A1 of the priority program 1640 ("joining by plastic deformation"); the authors would like to thank the German Research Foundation (DFG) for its financial support.

References

[1] Bellmann J., Lueg-Althoff J., Schulze S., Gies S., Beyer E., Tekkaya A.E.: *Measurement and analysis technologies for magnetic pulse welding: Established methods and new strategies*. Advances in Manufacturing, 2016, No. 4, pp. 322–339. http://dx.doi.org/10.1007/s40436-016-0162-5

[2] Bellmann J., Lueg-Althoff J., Schulze S., Gies S., Beyer E., Tekkaya A.E.: *Magnetic Pulse Welding: Solutions for Process Monitoring within Pulsed Magnetic Fields*. [in]: V. Otero (ed.), EAPPC & BEAMS & MEGAGAUSS 2016 – Proceedings 2016.

[3] Kapil A., Sharma A.: *Magnetic Pulse Welding: An efficient and environmentally friendly multi-material joining technique*. Journal of Cleaner Production, 2015, No. 100, pp. 35–58. http://dx.doi.org/10.1016/j.jclepro.2015.03.042

[4] Bellmann J., Kirchhoff G., Lueg-Althoff J., Schulze S., Gies S., Beyer E., Tekkaya A.E.: *Magnetic Pulse Welding: Joining within Microseconds –High Strength Forever*. [in]: American Welding Society and Japan Welding Society (ed.): *Proceedings of the 10th International Conference on Trends in Welding Research and 9th International Welding Symposium of Japan Welding Society*, 2016, pp. 91–94.

[5] Gies S., Löbbe C., Weddeling C., Tekkaya A.E.: *Thermal loads of working coils in electromagnetic sheet metal forming*. Journal of Materials Processing Technology, 2014, No. 11(214), pp. 2553–2565. http://dx.doi.org/10.1016/j.jmatprotec.2014.05.005

[6] Yablochnikov B.A., 2006 Patent US 7,015,435.

[7] Bellmann J., Lueg-Althoff J., Göbel G., Gies S., Beyer E., Tekkaya A.E.: *Effects of Surface Coatings on the Joint Formation During Magnetic Pulse Welding in Tube-to-Cylinder Configuration*. [in]: A.E. Tekkaya, M. Kleiner (eds.): ICHSF 2016: Proceedings of the 7th International Conference on High Speed Forming, 2016, pp. 279–288.

[8] Bellmann J., Lueg-Althoff J.: *Influence of Selected Coatings on the Welding Result During Magnetic Pulse Welding (MPW)*. [in]: Fraunhofer IWS Dresden (ed.): International Laser Symposium & International Symposium "Tailored Joining", 2016, Dresden, 2016.

[9] Seeberger, Datasheet AlMgSi (EN AW 6060), (accessed: 08.09.2016) http://www.seeberger.net/_assets/pdf/werkstoffe/aluminium/de/AlMgSi.pdf

[10] Günther + Schramm, Datasheet C45 (1.0503), (accessed: 08.09.2016) http://www.gs-stahl.de/files/datasheet/C45(1.0503).pdf

[11] DIN Deutsches Institut für Normung e.V.: *Load controlled fatigue testing –Execution and evaluation of cyclic tests at constant load amplitudes on metallic specimens and components*. 2016, Beuth Verlag GmbH, Berlin.

[12] Psyk V., Scheffler C., Drossel W.-G., Kolchuzhin V., Mehner J., Faes K., Zaitov O., van Bossche A.d., Bozalakov D.: *Advanced coil design for electromagnetic pulse technology – Report on the methodology of coil*

design: Ergebnisse des Vorhabens der industriellen Gemeinschaftsforschung (IGF) gefördert über die Arbeitsgemeinschaft industrieller Forschungsvereinigungen e.V. EFB-Forschungsbericht No. 397, Europ. Forschungsges. für Blechverarbeitung, Hannover, 2014.

[13] Verbraak A.C., Boes J.M., Chirer E.G., Visser L., Verkaik A. Patent US3305922 A.

[14] Fraunhofer IWS Dresden, Annual Report 2014.